Int. J. Heat Mass Transfer. Vol. 27, No. 9, pp. 1631–1640, 1984
Printed in Great Britain

0017–9310/84 $3.00 + 0.00

Direct contact condensation of vapor to falling cooled droplets

K. HIJIKATA, Y. MORI and S. KAWAGUCHI
Tokyo Institute of Technology, 2-12-1, Ohokayama, Meguro-ku, Tokyo, Japan

(*Received* 19 *October* 1983)

Abstract—Direct contact condensation of vapor to falling cooled droplets identical in material with the vapor has been investigated experimentally and theoretically to utilize the subcooled state of the condensed liquid for enhancing a high performance condenser, namely the condensate collected upon disks is sprinkled into the surrounding vapor in droplets and the vapor is condensed around them. Heat transfer of direct contact condensation to a droplet is rate-controlled by the heat transfer in the droplet. Experimental results obtained in this study show a heat transfer coefficient about ten times higher than that of the solid sphere and about four times higher than the theoretical value, considering the circulate motion in the spherical droplet. To explain this discrepancy, a theoretical analysis has been carried out with adequate consideration to the deforming oscillation of the droplet due to surface tension and it is clarified that the analytical solution well explains the experimental results.

INTRODUCTION

AN EFFECTIVE conversion of thermal energy with a small temperature difference from the ambient such as waste energy or ocean thermal energy to electric power is considered to be accomplished by a Rankine cycle using an organic compound as a working fluid. In the case of ocean thermal energy conversion (OTEC) the features are a very small difference between the high and low temperature heat sources of about 20°C and a very large amount of exhaust heat. Consequently, an increase of the cycle efficiency is required and can be realized by developing a high performance heat exchanger, especially a condenser. In addition to this, since the Freon used as a working fluid of the Rankine cycle is usually in the superheated state at the turbine exit, the condenser needs a high performance as a desuperheater. On the other hand, the condensed liquid is in the subcooled state. Therefore, in order to enhance the performance of the condenser, a fundamental study has been made in this paper to utilize this subcooled liquid for desuperheating the vapor, namely, the condensed liquid is dispersed into the vapor in droplets and the superheated vapor is directly condensed around them.

Generally, the main thermal resistance of the filmwise condensation heat transfer is heat conduction in the liquid film, and so augmentation of the heat transfer coefficient can be achieved by making the liquid film thin. To create the thin liquid film layer on the condensing surface, a vertical fluted tube shown in Fig. 1 with very low fins was used and the condensation mechanism was studied experimentally and analytically by the present authors [1, 2]. In this condensing tube, the liquid condensed on the tips of the tiny fins moved to the groove between each fin due to surface tension and then moved down the groove due to gravity. At the same time, the condensed liquid that moved down the groove was removed from the tube by disks set around the tube and the film thickness below the disk was made very thin.

In addition to this augmentation of heat transfer by surface tension, the enhancement of heat transfer was attempted by dispersing the liquid collected upon the disks into the vapor in droplets. As the first step to investigate this heat transfer enhancement by subcooled droplets, direct contact condensation of vapor to subcooled droplets that fall in the saturated vapor is studied experimentally.

According to the theoretical study, the condensation heat transfer of the falling droplet is rate controlled by the heat transfer in the droplet. The circulating motion in the droplet always exists by the shear stress at the surface. However, the convection has no effect because of the closed streamline, namely there is no temperature gradient along the streamline and the heat is only transferred across streamlines by conduction. On the other hand, if there is a deforming oscillation of the droplet, the mixing of fluid occurs between the different streamlines and the convection effect becomes predominant and the heat transfer coefficient increases. Therefore, the deforming oscillation of the falling droplet is very important from the standpoint of heat transfer enhancement. Brunson and Wellek [3]

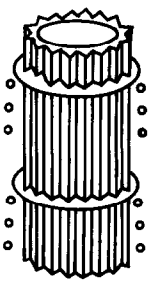

FIG. 1. A schema of the high performance vertical condensing tube.

NOMENCLATURE

a	thermal diffusivity of liquid [$m^2 s^{-1}$]	$U, \bar{V}$	time mean velocity [$m s^{-1}$]
C	constant	u, v'	fluctuation velocity [$m s^{-1}$]
C_0	$C\varepsilon_0^2\tilde{\omega}_0$		
C_p	specific heat at constant pressure [$J kg^{-1} K^{-1}$]	Greek symbols	
E	ratio of apparent heat and latent heat	ε	deformation rate of droplet
f	deforming oscillation frequency of droplet [Hz]	ε_0	amplitude of droplet deformation
L	latent heat [$J kg^{-1}$]	η	nondimensional distance, r/R
Nu	Nusselt number of droplet	λ	thermal conductivity of droplet [$W m^{-1} K^{-1}$]
Pe	Peclet number	ξ, ζ, ϕ	orthogonal coordinates in the droplet
q	heat flux [$W m^{-2}$]	ρ	density [$kg m^{-3}$]
R_0	initial droplet radius [m]	σ	surface tension [$N m^{-1}$]
r, θ	spherical coordinates	τ	nondimensional time, at/R_0^2
T	temperature [K]	ω_0	angular velocity of droplet deformation [s^{-1}]
T_m	volume average temperature in the droplet [K]	$\tilde{\omega}_0$	nondimensional angular velocity
T_s	saturation temperature [K]	Ω	nondimensional fluctuation velocity, uR_0/a.
t	time [s]		

investigated the oscillating droplet and reviewed previous studies, discussing analytical models at the same time. Even one of the most adequate models to explain the experimental results assumes a surface renewal model where a new surface with a mean droplet temperature appears at every cycle of the deforming oscillation, however, this model can not explain real physical phenomena. Using this model, it has been shown that our experimental results of heat transfer of oscillating droplets are four or more times larger than those of analytical results reported so far, for example, by Kronig and Brink [4], in which they gave consideration to the circulating motion in the droplet. In the theoretical study of this paper, a new model is proposed in order to take account of deformation of the droplet, particularly the second harmonic oscillation, and good agreement is shown to exist between the heat transfer experiments and the theoretical prediction.

EXPERIMENTAL STUDY

Experiment of condensation on a single droplet

The schematic diagram of the experimental apparatus is shown in Fig. 2. The test section is made of Pyrex glass of 76 mm I.D. and 750 mm length filled with saturated vapor. A subcooled liquid droplet identical in material to the vapor falls down the test section, causing condensation of the vapor upon it. Refrigerant R113 and methanol (CH_3OH) were used as the working material. The saturated vapor generated in the boiler goes through the superheater and enters the test chamber at the top. Vapor condensed on the inner wall of the chamber was gathered and returned to the boiler.

The subcooled liquid held in the pressurized tank was led to the droplet formation section through a water-jacketed small diameter tube of 0.2 mm I.D. and 200 mm length which controls its flow rate. The droplet was generated at the tip of a 1 mm I.D. needle set at the end of the tube and fell down into the chamber after a 0.1 mm copper–constantan thermocouple had measured its temperature.

The falling droplet was captured by a catcher which was movable in the vertical direction in the test chamber and the flow rate was measured by the volume caught in a unit time. The main part of the catcher is

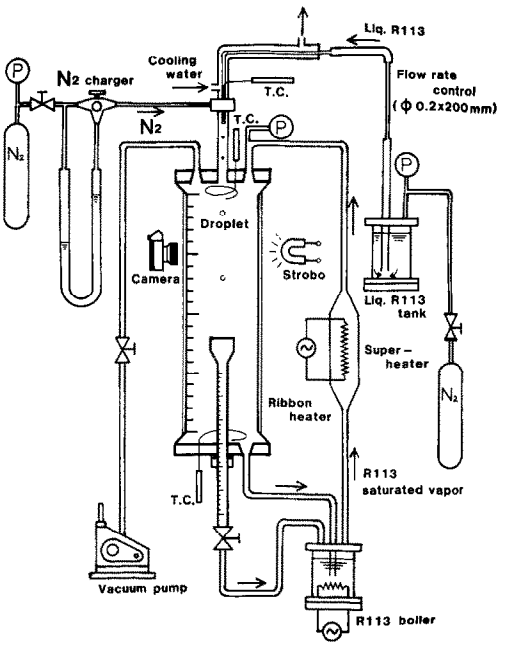

FIG. 2. A schematic diagram of the experimental apparatus.

made of a glass tube of 2 mm I.D. and 8 mm O.D. and the inlet part has an aluminum funnel so shaped to prevent unnecessary condensation after impingement of the droplet on the catcher. The center of the catcher tube is adjusted in such a way as to catch all of the falling droplets. The number of falling droplets per unit time was optically detected by a photo-transistor and the mean radius of the falling droplet at the catcher was calculated from the flow rate measured and the number of falling droplets. The falling velocity of the droplet was changed by changing the falling distance and, was measured by a photograph. A cylindrical space of small diameter was provided at the upper part of the chamber and was filled with a noncondensable gas for the reason stated below, and the droplet velocity at the bottom of the inlet space reached the terminal velocity of a falling droplet in the gravity field.

In order to prevent condensation of vapor on a droplet during the droplet formation at the needle tip and in the inlet space, the latter is made of a glass tube of 6 mm I.D. and 150 mm length and the noncondensable gas is filled in this section. Nitrogen and helium gases were selected as the noncondensable gas for the vapor of R113 and methanol, respectively, because the noncondensable gas must be lighter than the vapor. Since the noncondensable gas of smaller molecular weight than that of the vapor was accumulated in the small space of the inlet, the space which had a smaller diameter than that of the rest chamber, was cooled and the noncondensable gas gathered in the inlet space. Then, the stratified layers of the noncondensable gas and vapor were formed where the inlet space joins the test chamber with the introduction of a measured amount of noncondensable gas into the chamber. Figure 2 shows the combination system of R113 and nitrogen, while the same apparatus was used for the combination of methanol and helium.

First of all, the test section was evacuated and a vapor was generated by electrically heating the boiler to keep the system pressure constant. Then, a given amount of noncondensable gas was let in. Due to this procedure, it was possible to assume the starting point of condensation around a falling droplet at the top end of the test chamber. After the steady-state condition was reached, the experiment was carried out.

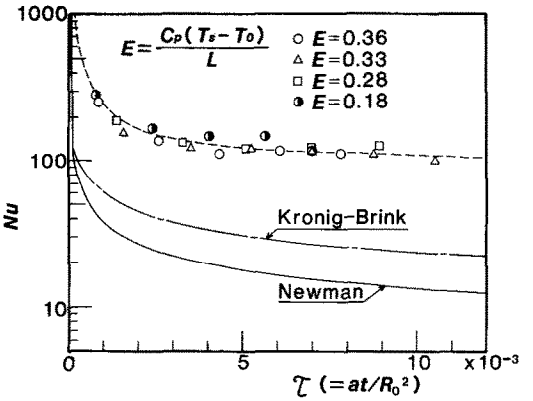

FIG. 4. Experimental results of Nusselt number for R113.

The typical radius change of the R113 droplet as it falls down the test chamber is shown in Fig. 3 where the abscissa shows the elapsed time of the droplet going in the perpendicular direction. The initial radius of $R = 0.925$ mm is calculated from the flow rate. The radius of $R = 1.015$ mm, indicated in the figure, is an equilibrium radius calculated from the energy balance using the initial droplet temperature and the difference between the initial droplet temperature and the saturation temperature of the vapor of 45 K. The ratio of the apparent heat and the latent heat is 0.33.

The variation of the volume-averaged temperature of the droplet with time was calculated from the droplet radius change with the assumption that the increase of the mean temperature came from the latent heat release of condensation. The measured changes of the Nusselt number with time obtained by these processes are shown in Figs. 4 and 5 for R113 and methanol, respectively. The initial radii are about 0.9 mm in each case and the abscissa shows the nondimensional elapsed time. In both cases of R113 and methanol, the Nusselt number is independent of the apparent latent heat ratio E, which means the heat transfer is controlled in the droplet, but not at the liquid–gas interface.

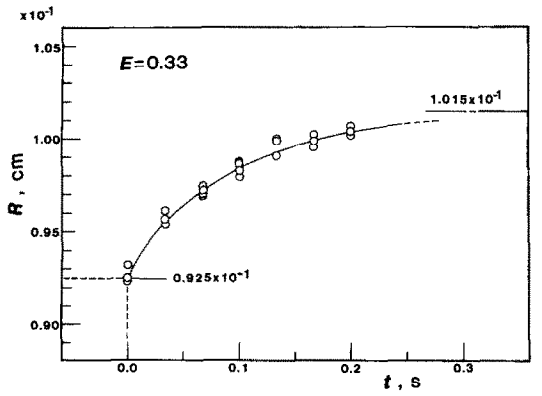

FIG. 3. Typical example of droplet radius change by condensation.

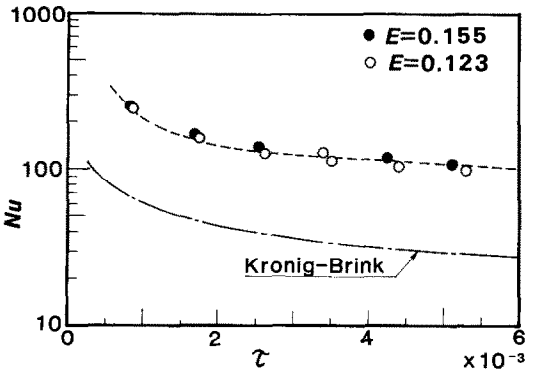

FIG. 5. Experimental results of Nusselt number for methanol.

Namely, the phase change process does not rate control this heat transfer phenomenon. The Nusselt number behavior with time obtained by experiments agrees qualitatively with that predicted by Kronig and Brink's theory which assumes the infinite circulation velocity in the droplet. However, the experimental results are four or more times larger than that by Kronig and Brink's solution. The Peclet number in the droplet under experimental conditions is estimated as about 2000 considering that the Reynolds number of the falling droplet is 10^4. The main causes of these differences are considered to be the following.

(1) The deformation of the droplet shape from the spherical one.
(2) The second-order harmonically deforming oscillation of the droplet.

To confirm these effects, high-speed photographs of falling droplets are taken and results are given below.

Behavior of falling droplet

The deformation shapes of the falling methanol droplet were taken with a high-speed camera and are shown in Fig. 6. The second-order harmonic oscillation of the droplet in its spherical shape is seen where the time interval of this oscillate motion is 25 ms (40 Hz). The frequency of deforming oscillation by surface tension is given by Lamb [5]. Neglecting the effect of the surrounding vapor density, it is as follows:

$$f = \left\{\frac{n(n-1)(n+2)}{4\pi^2 R_0^3 \rho}\right\}^{1/2}. \tag{1}$$

The theoretical frequency under the condition shown in Fig. 6 is $f = 39$ Hz and agrees well with the experimental one. For an R113 droplet, the frequency of 42 Hz obtained from the experiment also agrees well with the theoretical one of 43 Hz. To estimate the amplitude of the deforming oscillation, the largest deformed shape of the methanol droplet is shown in Fig. 7. The variation of the droplet in shape under the constant volume condition may be written as

$$R = R_0\{1+\varepsilon(t)(2\cos^2\theta - \sin^2\theta)\} \tag{2}$$

where R_0 is the time mean radius and ε is the deformation rate of the oscillation. The maximum value of ε is the nondimensional amplitude of the deforming oscillation and it is 0.12 for the methanol droplet shown in Fig. 7 and 0.13 for the R113 droplet. Thus the deforming oscillation of the droplet can be assumed to be the second harmonic oscillation in its spherical shape. A theoretical analysis given in the next section is carried out with consideration to the circulate

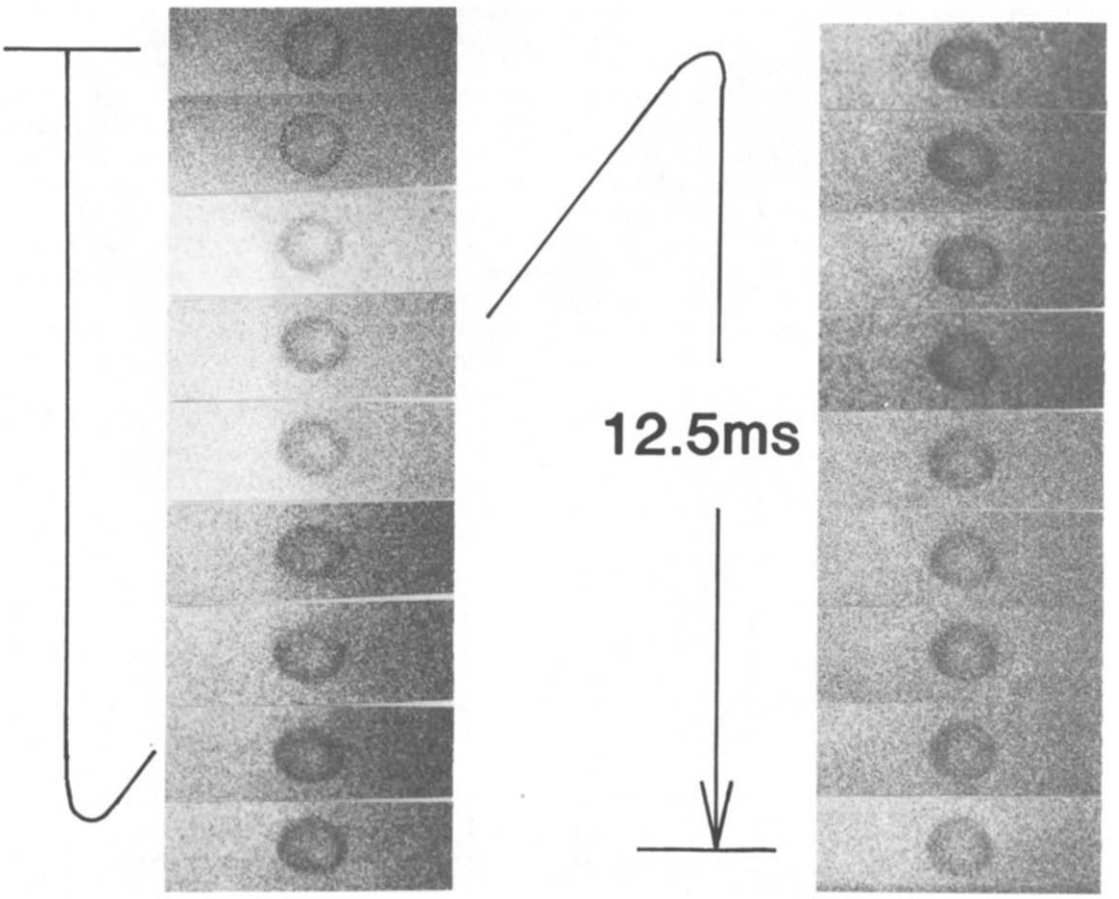

FIG. 6. Photographs of an oscillating methanol droplet.

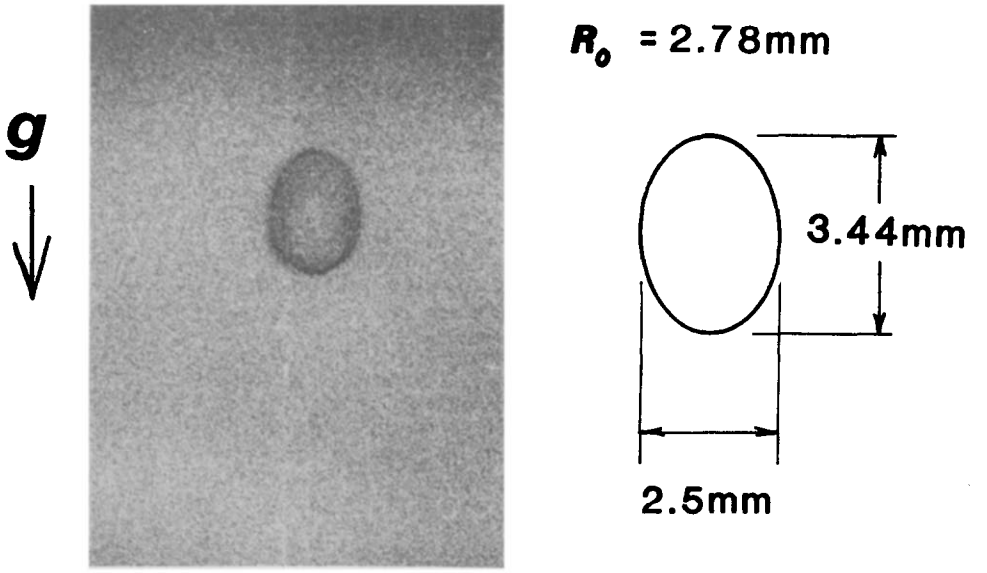

FIG. 7. Photographs of maximum deformation of a methanol droplet.

motion and the second-order harmonic oscillation of the droplet.

ANALYSIS

For the condensation of a one component saturated vapor, the saturation condition at the droplet surface is well assumed.

The energy equation in the droplet for the spherical coordinate (r, θ) is written as

$$\frac{\partial T}{\partial t}+v_r\frac{\partial T}{\partial r}+v_\theta\frac{\partial T}{\partial \theta_r}=a\left(\frac{1}{r^2}\frac{\partial}{\partial r}r^2\frac{\partial T}{\partial r}+\frac{1}{r^2}\frac{1}{\sin\theta}\frac{\partial}{\partial\theta}\sin\theta\frac{\partial T}{\partial\theta}\right). \quad (3)$$

Considering the circulate motion and deforming oscillation, the velocity distributions in the droplet are

$$v_r = U\cdot(1-r^2/R^2)\cos\theta+u(t)(3\cos^2\theta-1)r/R$$
$$v_\theta = -U\cdot(1-2r^2/R^2)\sin\theta-3u(t)\sin\theta\cos\theta(r/R). \quad (4)$$

The first terms of each velocity component show Hill's vortex motion and the second terms show the velocity caused by the oscillation. The velocity of oscillation is given by the deformation of the droplet

$$u(t)=R_0\frac{d\varepsilon}{dt}. \quad (5)$$

Since Hill's vortex is considered to be the zero-order motion, new orthogonal coordinates (ξ, ζ, ϕ), as shown in Fig. 8, are introduced, where the constant ξ line coincides with the circulating streamline and the constant ζ line is perpendicular to the constant ξ line and we have

$$\xi = 4(\eta^2-\eta^4)\sin^2\theta$$
$$\zeta = \eta^4\cos^4\theta/(2\eta^2-1) \quad (6)$$

where $\eta = r/R_0$.

The circle of radius $R_0/\sqrt{2}$ corresponds to $\zeta = \pm\infty$. In the inner region of this circle ζ has a negative value and in the outer region ζ is positive. From the experimental result indicating independency of the apparent and latent heat ratio E of the heat transfer coefficient, the effect of the radius increase by condensation can be ignored. By use of the new coordinates equation (3) can be rewritten as

$$\frac{\partial\tilde{T}}{\partial t}+h_\xi(Pe\,\bar{V}_\xi+\Omega v'_\xi)\frac{\partial\tilde{T}}{\partial\xi}+h_\zeta(Pe\,\bar{V}_\zeta+\Omega v'_\zeta)\frac{\partial\tilde{T}}{\partial\zeta}=A\left(\frac{\partial}{\partial\xi}\frac{h_\xi^2}{A}\frac{\partial\tilde{T}}{\partial\zeta}+\frac{\partial}{\partial\zeta}\frac{h_\zeta^2}{A}\frac{\partial\tilde{T}}{\partial\zeta}\right) \quad (7)$$

where, h_ξ, h_ζ and h_ϕ are the line elements along the (ξ, ζ, ϕ) coordinate and are written as

$$h_\xi^2 = (8\eta\sin\theta)^2\cdot\Delta$$
$$h_\zeta^2 = (4\eta^3\cos^3\theta)^2\cdot\Delta/(1-2\eta^2)^2 \quad (8)$$
$$h_\phi^2 = 1/(\eta\sin\theta)^2$$

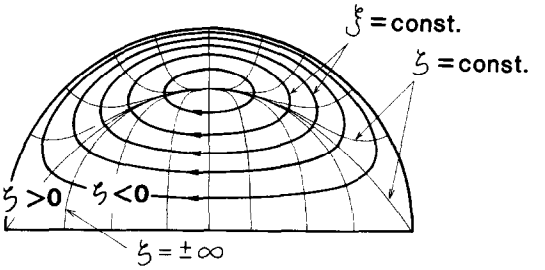

FIG. 8. An orthogonal coordinate in the droplet.

where

$$\Delta = (1-2\eta^2)^2 \sin^2\theta + (1-\eta^2)^2\cos^2\theta$$

$$A = h_\xi \cdot h_\zeta \cdot h_\phi \tag{9}$$

$$Pe = \frac{UR_0}{a}, \quad \tau = \frac{at}{R_0^2}, \quad \Omega = \frac{uR_0}{a}, \quad \bar{T} = \frac{T-T_0}{T_s-T_0}.$$

In equation (9) T_0 is the initial temperature of the droplet and Ω is the nondimensional velocity caused by the oscillation motion depending on time.

The velocities in the (ξ, ζ) coordinates are written as

$$\bar{V}_\xi = 0$$

$$h_\zeta \bar{V}_\zeta = -\frac{4\eta^3\cos^3\theta}{(1-2\eta^2)^2}\cdot\Delta = -\frac{1}{f} \tag{10}$$

$$v'_\xi = -\frac{\eta\sin\theta}{\sqrt{\Delta}}\{3\eta^2\cos^2\theta + (1-2\eta^2)\}.$$

$\bar{V}_\xi = 0$ means that there is no normal velocity component across the streamline without oscillation motion.

In consideration of the fact that the velocities consist of the mean values depending on Pe and the fluctuation terms containing Ω, the nondimensional temperature is also divided into the time mean value $\bar{T}$ and the fluctuation term T'. As Pe is large, the temperature is expanded by $1/Pe$

$$\bar{T} = (\bar{T}_0 + T'_0) + \frac{1}{Pe}(\bar{T}_1 + T'_1) + \ldots \tag{11}$$

where

$$[\int T'_i \, dt]_{\text{one cycle}} = 0.$$

Substituting equation (11) in equation (7) and taking time averaging during one oscillation cycle, we can get the equations of $O(Pe)$ and of $O(1)$ as follows

$$\bar{V}_\zeta \frac{\partial \bar{T}_0}{\partial \zeta} = 0$$

$$\frac{\partial \bar{T}_0}{\partial \tau} + h_\xi \overline{v'_\xi \Omega \frac{\partial T'_0}{\partial \xi}} + h_\zeta \bar{V}_\zeta \frac{\partial \bar{T}_1}{\partial \zeta} + h_\zeta \overline{v'_\zeta \Omega \frac{\partial T'_0}{\partial \zeta}} \tag{12}$$

$$= A\left(\frac{\partial}{\partial \xi}\frac{h_\xi^2}{A}\frac{\partial \bar{T}_0}{\partial \xi} + \frac{\partial}{\partial \zeta}\frac{h_\zeta^2}{A}\frac{\partial \bar{T}_0}{\partial \zeta}\right) \tag{13}$$

where bars indicate the time averaged value in a cycle. Equation (12) is obtained from the convection term of $\bar{T}_0$. From this equation, it is found that $\bar{T}_0$ is the only function of ξ, namely that the time mean temperature has a constant value along the circulating streamline. Equation (13) is integrated from $-\infty$ to $+\infty$ after being multiplied by f, and we get

$$\int_{-\infty}^{+\infty} f\frac{\partial \bar{T}_0}{\partial \tau}\, d\zeta + \int_{-\infty}^{+\infty} f h_\zeta v'_m \overline{\Omega \frac{\partial T'_0}{\partial \xi}}\, d\zeta + \int_{-\infty}^{+\infty} f h_\zeta v'_\zeta \overline{\Omega \frac{\partial T'_0}{\partial \zeta}}\, d\zeta - [\bar{T}_1]_{-\infty}^{+\infty} = \int_{-\infty}^{+\infty} f A \frac{\partial}{\partial \xi}\frac{h_\xi}{A}\frac{\partial \bar{T}_0}{\partial \xi} d\zeta. \tag{14}$$

As the line of constant ξ is closed in the droplet, the value at $\zeta = -\infty$ is equal to the values at $\zeta = +\infty$. Therefore, the fourth term on the LHS of equation (14) becomes zero.

The continuity equation is rewritten as

$$A\left(\frac{\partial}{\partial \xi}\frac{h_\xi}{A}v'_\xi\Omega + \frac{\partial}{\partial \zeta}\frac{h_\zeta}{A}v'_\zeta\Omega\right) = 0. \tag{15}$$

After multiplying equation (15) by f, averaging it in one oscillation cycle and integrating it from $-\infty$ to $+\infty$ with respect to ζ, the equation thus obtained is added to equation (14) and rearranged by use of the relation $f \cdot A = 8$, we have

$$\frac{\partial \bar{T}_0}{\partial \tau}\int_{-\infty}^{+\infty} f\, d\zeta + \int_{-\infty}^{+\infty} 8\frac{\partial}{\partial \xi}\frac{h_\xi \overline{v'_\xi \Omega T'_0}}{A}\, d\zeta + 8\left[\frac{h_\zeta \overline{v'_\zeta \Omega T'_0}}{A}\right]_{-\infty}^{+\infty} = \int_{-\infty}^{+\infty} 8\frac{\partial}{\partial \xi}\frac{h_\xi^2}{A}\frac{\partial \bar{T}_0}{\partial \xi} d\zeta. \tag{16}$$

The third term on the LHS also becomes zero because the constant ξ lines are closed in the droplet.

To solve equation (16) the correlation between Ω and T'_0 needs to be assumed. In this study the correlation of $\overline{\Omega T'_0}$ is related to the time mean temperature gradient by use of the same model of turbulent mixing

$$\bar{T}'_0 \propto -\left\{\frac{\Omega v'_\xi}{d(\ln \Omega v'_\xi)/d\tau}\right\} \cdot \text{grad}\ \bar{T}_0. \tag{17}$$

In equation (17) the numerator $(\Omega v'_\xi)$ is the fluctuation velocity across the time mean streamline, the denominator $(d(\ln \Omega v'_\xi)/d\tau)$ is the angular velocity of the fluctuation and the term in the brackets is the displacement of the instantaneous streamline from the time mean streamline. Therefore, the temperature fluctuation is considered to be proportional to the product of the mean temperature gradient and the characteristic displacement length of the deforming oscillation. Substituting equation (17) in equation (18) and expressing the amplitude and angular velocity of the deforming oscillation with ε_0 and ω_0, respectively, we have

$$\frac{\partial \bar{T}_0}{\partial \tau}\int_{-\infty}^{+\infty} f\, d\zeta = \int_{-\infty}^{+\infty} 8\frac{\partial}{\partial \xi}\left\{\frac{h_\xi^2}{A} + \frac{h_\xi^2}{A} C\varepsilon_0^2 \times \left(\frac{R_0^2\omega_0}{a}\right)v'^2_\xi\right\}\frac{\partial \bar{T}_0}{\partial \xi}\, d\zeta \tag{18}$$

where C is the proportional constant in equation (17). The LHS of equation (18) is the unsteady term and the first and second terms on the RHS are the diffusion term and the mixing term by the oscillation motion, respectively. When the integrated values in equation (18) are expressed by $q(\xi)$, $p(\xi)$ and $n(\xi)$, then these

variables are rewritten as

$$q(\xi) = \int_{-\infty}^{+\infty} f\,\mathrm{d}\zeta = \int_{-\infty}^{+\infty} \frac{(1-2\eta^2)^2}{4\eta^3\cos^3\theta\cdot\Delta}\,\mathrm{d}\zeta$$

$$p(\xi) = \int_{-\infty}^{+\infty} \frac{h_\xi^2}{2A}\,\mathrm{d}\zeta = \int_{-\infty}^{+\infty} \frac{\sin^2\theta(1-2\eta^2)^2}{\eta\cos^3\theta}\,\mathrm{d}\zeta$$

$$n(\xi) = \int_{-\infty}^{+\infty} \frac{h_\xi^2}{2A} v_\xi'^2\,\mathrm{d}\zeta$$

$$= \int_{-\infty}^{+\infty} \frac{\sin^4\theta(1-2\eta^2)^2}{\Delta\cos^3\theta} \times\{3\eta^2\cos^2\theta+(1-2\eta^2)\}^2\,\mathrm{d}\zeta. \quad (19)$$

Equation (18) is rewritten by using these variables in the following form

$$q(\xi)\frac{\partial\bar{T}_0}{\partial\tau} = 16\frac{\partial}{\partial\xi}\{p(\xi)+C_0 n(\xi)\}\frac{\partial\bar{T}_0}{\partial\xi} \quad (20)$$

where

$$\bar{\omega}_0 = R_0^2\omega_0/a, \quad C_0 = C\varepsilon_0^2\bar{\omega}_0.$$

Equation (20) is the fundamental equation of the heat transfer in the droplet with deforming oscillation. C_0 that appears in the mixing term is a parameter that indicates the strength of mixing and is macroscopically related to the amplitude and frequency of oscillation. To calculate the values of $p(\xi)$, $q(\xi)$ and $n(\xi)$, a new independent variable $y = \eta^2$ is introduced

$$q(\xi) = \frac{1}{2}\int_{y_1}^{y_2}\frac{\mathrm{d}y}{J(y)}$$

$$p(\xi) = \frac{\xi}{2}\int_{y_1}^{y_2}\frac{(1-y)^3-\xi(2-3y)/4}{(1-y)^2J(y)}\,\mathrm{d}y \quad (21)$$

$$n(\xi) = \frac{\xi^2}{8}\int_{y_1}^{y_2}\frac{(1-y^2-0.75\xi)^2}{(1-y)^4J(y)}\,\mathrm{d}y$$

where

$$J(y) = \sqrt{((1-y)(y-y_1)(y_2-y))}$$
$$y_1 = (1-\sqrt{(1-\xi)})/2$$
$$y_2 = (1+\sqrt{(1-\xi)})/2. \quad (22)$$

The values of $p(\xi)$, $q(\xi)$ and $n(\xi)$ are obtained by numerical integrations and are shown in Fig. 9. $\xi = 1$ is the center of Hill's vortex motion and $q = \pi/\sqrt{2}$, $p = 0$ and $n = 0$ at that point. On the other hand, $\xi = 0$ is the surface of the droplet where $q = -(\ln\xi)/2$, $p = 8/3$ and $n = 32/21$. The values of p, q and n monotonously decrease with an increase of ξ. At the center of Hill's vortex, there is no heat flux by diffusion and mixing because of n and p are zero.

The solution of equation (20) at $\tau = \infty$ is obtained by assuming $\bar{T}_0$ to be $\hat{T}_0\cdot\exp(-\alpha\tau)$ under the following conditions

$$\xi = 0: \quad \hat{T}_0 = 0$$
$$\xi = 1: \quad \partial\hat{T}_0/\partial\xi = 0 \quad (23)$$

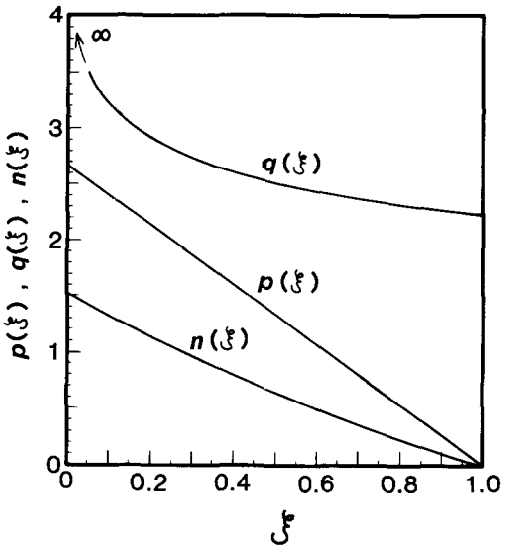

FIG. 9. Variations of $p(\xi)$, $q(\xi)$ and $n(\xi)$ with ξ.

where α is the eigenvalue of equation (20). In this case, the Nusselt number is given by equation (24) by using the droplet diameter $2R_0$ as the characteristic length and the temperature difference between the saturation temperature and initial temperature $(T_s - T_0)$ as the characteristic temperature difference

$$Nu = \frac{\frac{4}{3}\pi R_0^3\cdot C_p\rho\left(\frac{\partial T_m}{\partial t}\right)\cdot 2R_0}{4\pi R_0^2\lambda\cdot(T_s-T_m)} = -\frac{2}{3}\cdot\left(\frac{\mathrm{d}\ln\bar{T}_0}{\mathrm{d}\tau}\right) = \frac{2}{3}\alpha. \quad (24)$$

The Nusselt number at $\tau = \infty$ thus obtained is plotted in Fig. 10 as a function of C_0. The Nusselt number increases linearly with an increase of C_0. The value at $C_0 = 0$ corresponds to the solution obtained using Kronig and Brink's method where the deforming

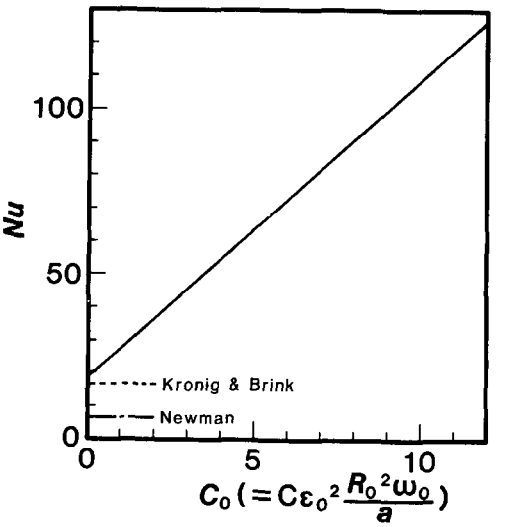

FIG. 10. Nusselt number at $\tau = \infty$.

Table 1. Values of C_0, ε_0 and $\tilde{\omega}_0$

	R113	CH_3OH
ε_0	0.13	0.12
ω_0	7000	7000
C_0	11.8	10.1

oscillation effect is considered. However, the Nusselt number obtained in this study has about a 10% higher value than that of Kronig and Brink's solution. The cause of this discrepancy is considered to be due to the inaccuracy of Kronig and Brink's solution because they only obtained the second-order solution by Ritz's method.

The time-dependent solution of equation (20) is obtained by numerical calculation of the time marching method. These numerical results are compared with the experimental results in the following section.

The proportional constant C contained in the parameter C_0 in equation (20) to calculate α is unknown; however, it corresponds to the constant C_μ/σ_t which appears in the model of two equations in the turbulent flow analysis, where C_μ is the proportional constant between the eddy viscosity and the value of the square of the turbulent kinetic energy divided by the turbulent dissipation and σ_t is the turbulent Prandtl number. In the turbulent flow, mixing of temperature is caused by turbulent motion, however, a similar mixing process appears in the droplet even in the laminar flow region, because the instantaneous streamline is not closed but crosses each other in the deforming oscillation. Therefore, by adopting values in turbulent mixing, for those constants such as $C_\mu = 0.09$ and $\sigma_t = 0.9$, C is given as 0.1. By Using this value of C and the experimental values of ε_0 and $\tilde{\omega}_0$, C_0 can be calculated. They are tabulated in Table 1, along with the values of ε_0 and $\tilde{\omega}_0$. The values of C_0 are 11.8 and 10.1 for R113 and methanol, respectively.

COMPARISON BETWEEN THEORY AND EXPERIMENT

The experimental results with R113 and methanol shown in Figs. 4 and 5 are compared with the theoretical results shown by solid lines in Figs. 11 and 12, respectively. The theoretical value of the Nusselt number rapidly decreases with an increase of τ in the region of $\tau < 0.001$ and becomes constant at $\tau > 10$. The theoretically calculated values of Nusselt number with time are seen to be in good agreement with the experimental results. By using ε_0 obtained from the measurement amplitude of oscillation the theoretical values for Fig. 11 are calculated by taking $C_0 = 10$ and 12, while for Fig. 12, $C_0 = 10$. These values are consistent with the predicted values given in the preceding section. The nondimensional values of ε_0 and $\tilde{\omega}_0$ for R113 are nearly equal to those for methanol, whereas the physical properties used in these

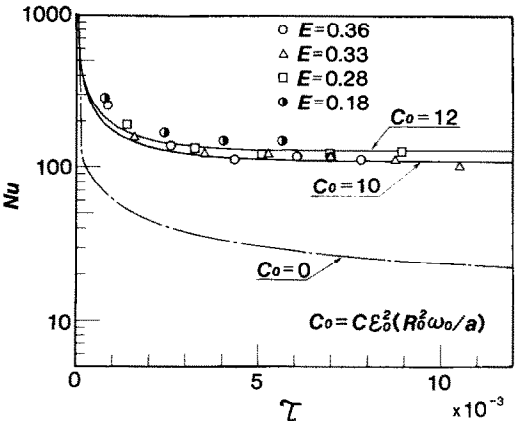

FIG. 11. Comparison between theory and experiment of Nu for R113.

nondimensional values are quite different from each other as shown in Table 2.

These analytical results well explain the experimental Nusselt number values except for a small τ region. This discrepancy in the very small τ region is considered to be caused by the inaccuracy of dR/dt and ε_0, because, the change of radius is very rapid and the measurement of dR/dt is less accurate than that of R in the small τ region. In addition to this reason, the value of ε_0 used is determined from the value measured at the middle of the test section. As the deforming oscillation of the droplet is generated when it leaves the nozzle and its amplitude monotonously decreases with increase of time, the real value of ε_0 in the smaller τ region is considered larger than that used in the analysis. At any rate, the theoretical result can well explain the measured high heat transfer rate of the oscillating droplets.

To end up, the characteristic of this analysis is summarized. Since every streamline of the circulating motion closes everywhere and the temperature is constant along the streamline without deforming oscillation, the heat is transferred only by conduction across the streamlines. Therefore, the increase of the heat transfer coefficient is caused by the increase in area

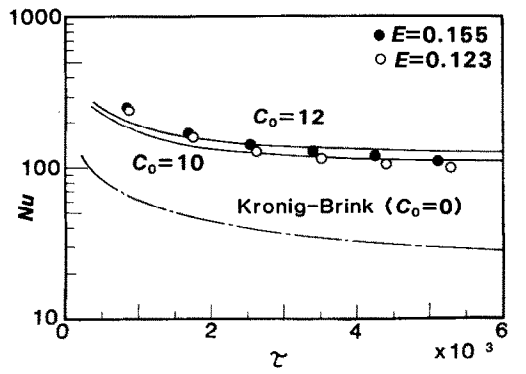

FIG. 12. Comparison between theory and experiment of Nu for methanol.

Table 2. Physical properties of R113 and methanol

		R113	CH_3OH
a	$[m^2 s^{-1}]$	5.08×10^{-8}	1.08×10^{-7}
C_p	$[kJ kg^{-1} K^{-1}]$	0.95	2.47
L	$[kJ kg^{-1}]$	155	1170
λ	$[W m^{-1} K^{-1}]$	0.075	0.20
ρ	$[kg m^{-3}]$	1580	790
σ	$[N m^{-1}]$	1.9×10^{-2}	2.2×10^{-3}

that has the same temperature and it corresponds to the difference between the solutions of Newman and Kronig and Brink as shown in Fig. 4. On the other hand, the droplet generated by ejection from a needle or a nozzle is oscillating by surface tension after leaving the tip of it. In this case, the time mean streamlines are closed but instantaneously the streamlines cross each other and convective heat transfer gets very effective. This is the cause of the very high heat transfer coefficient.

The convection effect caused by the deforming oscillation of the droplet is expressed by the velocity fluctuation perpendicular to the time mean streamlines (direction of ξ), as shown by the second term on the LHS of equation (8). Usually, v'_ξ is negligible, compared with the time mean velocity. However, in this case, as $\bar{V}_\xi = 0$ and $dT_0/d\xi$ is large, the contribution of this term on the heat transfer coefficient is very important.

CONCLUSIONS

The experimental and theoretical investigations are carried out using R113 and methanol on direct contact condensation of vapor to the falling cooled droplet of the same material as the vapor. The following conclusions are obtained.

(1) The experimental results of direct contact condensation heat transfer to the falling droplet show a very high heat transfer rate and is four or more times larger than the analytical results obtained by Kronig and Brink.

(2) The falling droplet has not a steady spherical shape, but oscillates with the second harmonically deforming motion by surface tension.

(3) An analytical study is carried out with consideration to the second-order harmonically deforming oscillation and the circulating motion in the droplet. The analytical study shows that the heat transfer coefficient increases with an increase of the oscillation amplitude.

(4) The analytical solution well explains the experimental results. However, it is a problem for the future to analytically determine the amplitude of the droplet oscillation.

Acknowledgement—The authors acknowledge the financial support of the Grant-in-Aid for Scientific Research (Nos. 505011, 56040052, 57040036) of the Ministry of Education, Japan.

REFERENCES

1. Y. Mori, K. Hijikata, S. Hirasawa and W. Nakayama, Optimized performance of condensers with outside condensing surface, *Trans. Am. Soc. Mech. Engrs*, Series C, *J. Heat Transfer* **103**(1), 96–102 (1981).
2. S. Hirasawa, Y. Mori, K. Hijikata and W. Nakayama, Optimum surface shape of vertical condensing tube (in Japanese), *Trans. Japan Soc. Mech. Engrs* **48**(427), 527–535 (1952).
3. R. J. Brunson and R. M. Wellek, Mass transfer within oscillating liquid droplet, *Can. J. Chem. Engng* **48**, 267–274 (1970).
4. R. Kronig and J. C. Brink, On the theory of extraction from falling droplets, *Appl. Scient. Res.* **A2**, 142–155 (1949).
5. Sir H. Lamb, *Hydrodynamics*. Cambridge University Press, London (1932).

CONDENSATION PAR CONTACT DIRECT D'UNE VAPEUR AVEC DES GOUTTELETTES TOMBANTES FROIDES

Résumé—La condensation par contact direct d'une vapeur avec des gouttelettes tombantes froides et de même composition est étudiée expérimentalement et théoriquement pour utiliser l'état sous-refroidi du liquide condensé à l'amélioration d'un condenseur à haute performance; le condensat collecté sur des disques est dispersé dans la vapeur environnante en gouttelettes et la vapeur est condensée autour d'elles. Cette condensation est limitée par le transfert thermique dans la gouttelette. Des résultats expérimentaux de cette étude montrent que le coefficient de transfert thermique est environ dix foix plus grand que pour une sphère solide et environ quatre fois plus élevé que la valeur théorique qui suppose le mouvement circulaire de la gouttelette sphérique. Pour expliquer cet écart, l'étude théorique suppose une oscillation de déformation de la gouttelette due à la tension interfaciale et cela montre clairement que la solution analytique explique bien les résultats expérimentaux.

DAMPFKONDENSATION DURCH DIREKTEN KONTAKT MIT FALLENDEN UNTERKÜHLTEN TROPFEN

Zusammenfassung—Die Kondensation von Dampf in direktem Kontakt mit fallenden unterkühlten Tropfen desselben Stoffes wurde experimentell und theoretisch untersucht. Der unterkühlte Zustand der Flüssigkeit wird genutzt, die Leistung des Kondensators zu erhöhen. Das Kondensat wird auf Scheiben aufgegeben und in Tropfen in den umgebenden Dampf versprüht, der dann an den Tropfen kondensiert. Der Wärmeübergang in direktem Kontakt wird durch den Wärmetransport im Tropfen bestimmt. Die experimentellen Ergebnisse dieser Untersuchung zeigen einen etwa zehnmal höheren Wärmeübergangskoeffizienten bei Tropfen gegenüber massiven Kugeln und einen etwa viermal höheren gegenüber dem theoretischen Wert, wenn man die zirkulierende Bewegung eines kugeligen Tropfens betrachtet. Um diese Diskrepanz zu erklären, wurden theoretische Untersuchungen mit adäquater Betrachtung der deformierenden Schwingungen des Tropfens infolge der Oberflächenspannung durchgeführt, und es zeigt sich, daß die analytische Lösung gut mit experimentellen Ergebnissen übereinstimmt.

ПРЯМАЯ КОНТАКТНАЯ КОНДЕНСАЦИЯ ПАРА НА ПАДАЮЩИХ ОХЛАЖДЕННЫХ КАПЛЯХ

Аннотация—Экспериментально и теоретически исследовалась прямая контактная конденсация пара на падающих охлажденных каплях той же жидкости, чтобы выяснить возможность использования недогретого конденсата для повышения к.п.д. конденсатора за счет разбрызгивания его диском в окружающий пар, снова конденсирующийся на каплях. Теплоперенос при прямой контактной конденсации определяется интенсивностью теплопередачи в самих каплях. По полученным опытным данным коэффициент теплопереноса почти на порядок больше, нежели для твердой сферы, и примерно в четыре раза превышает расчетную величину, учитывающую циркуляцию жидкости в сферической капле. Из специального теоретического анализа с аналогичным учетом деформационных пульсаций капель из-за поверхностного натяжения получено хорошее согласование аналитического решения с опытными данными.